Journal of Materials Chemistry C

ROYAL SOCIETY OF CHEMISTRY

PAPER

View Article Online
View Journal | View Issue

Cite this: J. Mater. Chem. C, 2024, 12, 12882

Low-temperature sintering of Cu@Ag microparticles in air for recyclable printed electronics†

David van Impelen, [a] Lola González-García *[ab] and Tobias Kraus *[ac]

Silver-coated copper microparticles combine the oxidation resistance of silver with the low cost of copper. They are interesting components for printed conductive structures. We studied whether printed films of such particles can be printed and sintered at low temperatures in air to create highly conductive films and whether it is possible to recover the particles from them for recycling. Pastes containing 1.5 μm to 5 μm spheres and 3 μm flakes with L-ascorbic acid were prepared, screen-printed, and treated at temperatures of 110 °C to 300 °C in air. The bulk resistance of films treated below 160 °C were two orders of magnitude higher than that of bulk copper, ρ_{Cu}, and limited by particle–particle contact resistances. They were reduced by treating the prints at 160 °C to 250 °C, leading to bulk film resistances down to $41\rho_{Cu}$. We demonstrate that the high mobility of silver enables the formation of necks that bridge the copper cores and reduce resistivity in this temperature window. The sintered prints retained their conductivity for at least 6 months. Treatments at higher temperatures in air were detrimental: resistances increased above 250 °C. These temperatures led to dewetting of the silver coating and fast copper oxidation, resulting in a continuously increasing resistance. In a final study, we demonstrated that films treated below 200 °C can be recycled by recovering the metal powder from the printed conductors and that the powder can be printed again.

Received 16th May 2024,
Accepted 16th July 2024

DOI: 10.1039/d4tc02028f

rsc.li/materials-c

1 Introduction

Silver-based conductive pastes dominate printed electronics due to their excellent conductivity,[1] their resistance to oxidation,[2] and their ability to withstand high temperatures.[3,4] Printable pastes are typically composed of silver particles dispersed in a binder matrix and can be employed to create highly conductive connections when screen-printed. Nonetheless, the high cost of silver and its limited global availability[5] pose economic challenges for industries reliant on silver-based electronic materials. Silver mining and extraction processes have large ecological impacts.[6] Recycling silver from prints can thus be economically and ecologically beneficial. Kwon *et al.* demonstrated an approach to recycling silver micro flakes from a printed conductor and reusing the flakes to print new conductors without losing performance.[7]

Besides the interest in recycling the silver used in printed conductors, there is also a growing interest in replacing silver-based pastes with cheaper, more sustainable, and readily available alternatives. Copper has a high conductivity,[8] is cheaper than silver,[9,10] and more abundant.[5,11] Therefore, many attempts have been made to replace silver with copper particles in conductive pastes.[12,13] The challenge with copper, however, arises from copper's tendency to form electrically insulating oxides in air[14–16] and the fact that copper particles typically require a higher sintering temperature than silver despite of the comparable melting points.[12,13] Printed copper conductors are usually treated at temperatures above 250 °C in nitrogen or reducing atmosphere, which increases cost.

Copper has two stable oxide phases, namely Cu_2O and CuO. A clean copper surface oxidizes readily in air at ambient conditions to form a thin native oxide layer with a thickness of a couple of nanometers.[17–19] This native oxide layer passivates the copper surfaces, preventing further growth. There is consensus in the literature that the main component of the native oxide is Cu_2O;[17] some groups claim the presence of CuO.[18,19] Since copper oxides are electrically insulating, the native oxide layer affects the conduction across interfaces. The electrical conductivities of copper thin films degrade when the temperature is increased in air such that the self-limiting

[a] INM - Leibniz-Institute for New Materials, Campus D2 2, 66123 Saarbrücken, Germany
[b] Saarland University, Department of Materials Science and Engineering, Campus D2 2, 66123 Saarbrücken, Germany. E-mail: lola.gonzalez-garcia@leibniz-inm.de
[c] Saarland University, Colloid and Interface Chemistry, Campus D2 2, 66123 Saarbrücken, Germany. E-mail: tobias.kraus@leibniz-inm.de

† Electronic supplementary information (ESI) available. See DOI: https://doi.org/10.1039/d4tc02028f

diffusion barrier of the native oxide layer fails.[14] Choudhary *et al.* found that films with thicknesses between 100 and 1000 nm[14] formed an amorphous Cu_2O phase on top of the native oxide layer at 150 °C that strongly increased their sheet resistances.

Conductive films of printed copper particles suffer more severely from the native oxide layer. The high specific surface area of copper powders renders them non-conductive after printing. Sintering can increase conductivity by forming metallic necks between particles, but the native oxide hinders efficient sintering below 400 °C.[20] Strategies to reduce the sintering temperature include polymer surfactants,[21,22] coating particles with metals,[13,22] and additives in paste formulations.[16,20]

The addition of L-ascorbic acid (AA, vitamin C) to copper-based paste formulations can suppress the oxidation of copper.[16,20] Gao *et al.* investigated this effect of AA addition on the sintering of copper microparticles. Firstly, they printed a paste of copper particles with diameters from several nanometers to 500 nm on a copper substrate, placed a copper chip onto it, and sintered the paste to create sintered joints. They found that copper oxides that formed during sintering blocked diffusion at the particle–particle and particle–substrate interfaces and hindered sintering. Incomplete sintering and weak bonds were the result at 350 °C in nitrogen. The addition of AA increased bonding strength[20] by reducing Cu_2O to Cu^0 and preventing further oxidation during sintering by scavenging oxygen. Pacioni *et al.* used UV-visible and electron paramagnetic resonance (EPR) spectroscopy to demonstrate that AA slows down oxidation by reducing copper ions to Cu^0. Gao *et al.* reports that AA is scavenging oxygen through its own oxidation.[16]

A complementary strategy is to prevent copper particle oxidation with thin silver coatings. They suppress oxidation at room temperature in air for at least 6 months.[13,22] Choi *et al.* performed thermogravimetry on 2 μm diameter pure copper and silver-coated copper particles in air at 10 °C min^{-1} and found an increase in the onset of oxidation from 148 to 220 °C.[23] Yu *et al.* found an increase for 50 nm diameter copper nanoparticles with and without silver shell from 85 to 157 °C.[24] Dewetting limits the protective effect of silver: Hai *et al.* studied 2 μm diameter silver-coated copper particles with a 260 nm thick silver coating and found that dewetting ensued at 200 °C.[25] The oxidation of the copper core was a result of dewetting, which exposed the copper surface and immediately oxidized in air. Kim *et al.* showed that oxidation can even set in before dewetting.[26] A 100 nm thick copper film coated with a 10 nm silver layer exposed to air at 250 °C formed a Cu_2O phase on top of the silver coating, as revealed by cross-sectional transmission electron microscope (TEM) imaging. Copper atoms diffused through the thin silver layer to form Cu_2O at the air-exposed surface.

Silver-coated copper particles have been used in printed conductive layers[24,27–34] and to achieve sinter bonding of integrated circuits for power electronics applications.[35–39] Świerzy *et al.* synthesized 1 μm -diameter microparticles with copper cores and 20 nm-thick silver shells.[27] Pastes were formulated, printed, and treated at 250 °C in nitrogen for 15 min to create conductive prints. In later work, the authors used propionic, oxalic, citric, or oleic acid to chemically increase the conductivity of the prints.[28] Kim *et al.* prepared Cu@Ag nanoparticles with diameters ranging from 200 to 900 nm (average diameter of 450 nm).[30] Pastes containing these particles were screen printed and treated at 200 °C in nitrogen for 60 min to reach 8.2 μΩ cm. Zhang *et al.* screen-printed elliptic silver-coated nanoflakes that were treated at 150 °C in nitrogen for 2 h and reached 37.5 μΩ cm.[34]

The sintering of silver-coated copper particles has been studied, too. It affects the conductivity of printed layers. Yu *et al.* synthesized 50 nm-sized silver-coated copper particles and sintered them in nitrogen at 350 °C.[24] Dewetting set in at 156 °C, sintering of the silver coating at 200 °C, and sintering of the copper cores at 250 °C. Kim *et al.* sintered 351 nm diameter silver-coated copper particles under isostatic pressure at 350 °C and 10 MPa.[40] The particles formed silver necks before the copper cores started to sinter.

Previous work on printed conductive layers of silver-coated copper particles relied on nitrogen, high temperatures, and/or high isostatic pressures applied on the prints. In this manuscript, we show that low-temperature treatments of such particles can yield relevant conductivities even in ambient air. We used L-ascorbic acid to suppress the oxidation of copper and avoided silver dewetting. We discuss the low-temperature sintering mechanisms that formed conductive silver necks bridging the copper cores. Furthermore, we demonstrate that the weakly sintered particles can be recovered from prints and the recovered powder directly reused.

2 Materials and methods

2.1 Preparation and printing of pastes

Commercial atomized silver-coated copper spheres (10% Ag coated Cu-HWQ, Fukuda Metal Foil and Powder Co., Ltd, Japan) with average diameters of 1.5, 3, and 5 μm, and commercial atomized silver-coated copper flakes (AgCu 0204C-12 Flake, Ames Goldsmith, United Kingdom) with an average diameter of 3 μm were used to formulate screen printing pastes. The diameter of the flakes was calculated by the manufacturer from laser diffraction results assuming the particles to be spherical. We will refer to this diameter in the remainder of this manuscript as equivalent diameter. The respective dry powder was mixed with ethylene glycol (EG, anhydrous 98%, Sigma Aldrich) at a weight ratio of 8 : 1 (Cu@Ag : EG, 1.5, 3 μm spheres, and flakes) or 8.5 : 1 (Cu@Ag : EG, 5 μm spheres) using a bladeless mixer (SpeedMixer DAC 150.3 SP, Hauschild, Germany) at 2350 rpm for 3 min, resulting in a highly viscous paste.

Lines of 1 × 3 cm^2 were screen-printed with a manual screen printer using a mesh of 120 polyester threads per centimeter on microscopy glass slides (VWR, ground edge frosted, Germany). The film thicknesses (average of 3 samples) were measured with a 3D confocal microscope MarSurf CM explorer (Mahr, Germany), and

found to be 24.5 ± 1.5, 38.6 ± 5.3, and 74.0 ± 7.8 μm (mean ± standard deviation) for prints containing 1.5, 3, and 5 μm diameter coated spheres, and 24.9 ± 0.6 μm for prints of coated flakes. After printing, the samples were immediately placed on a hotplate with closed lit (PZ28-3TD, Präzitherm, Germany) coupled to a PID controller (PR5-3T, Präzitherm, Germany) for 30 min set to the temperatures given in the main text and then cooled down in ambient air. The specified 'spread of temperature' across the hotplate is ±2 °C, and the lid suppresses convection and ensures minimal surface-normal temperature gradients. Three samples were prepared for each heat treatment. After the heat treatments, the samples were stored in laboratory air where the temperature was kept around 20 °C and humidity below 50%.

2.2 Characterization methods

The internal structures of particles and prints were analyzed using cross sections prepared by creating a trench in prints using a focused ion beam (FEI Versa 3D DualBeam) and imaging using scanning electron microscopy (SEM, Quanta 400 ESEM, Thermo Fisher Scientific GmbH, Germany) with the secondary electron detector.

The electrical conductivities of the printed lines were quantified immediately after the samples had cooled down with a four-point probe set up using a 2450 Sourcemeter (Keithley Instruments, Ohio, USA) using four in-line conical gold pins (GKS-069 201 051 A 0700, Ingun, Germany) with pin-to-pin distances of 1 mm.

Certain samples were electrically characterized *in situ* during the heat treatment using a two-point connection. The printed samples were dried for at least 2 days in vacuum at room temperature and then connected using copper wires at both ends of the printed line using conductive silver paste (G3692, Plano GmbH, Wetzlar, Germany) for the 90 and 110 °C treatments and conductive epoxy (Duralco 124, high temperature stable conductive silver epoxy from Polytec PT, Karlsbad, Germany) for all other temperature treatments. The epoxy glue was treated in a vacuum for 30 min before the start of the experiment. The samples were connected to a multichannel sourcemeter (DAQ6510 data acquisition logging multi-meter system) equipped with multiplexer cards (7702 40-channel differential multiplexer module with screw terminals) from Keithley Instruments GmbH (Germering, Germany) and mounted on a preheated programmable hot plate using Kapton tape (Plano GmbH, Wetzlar, Germany). A constant voltage bias of 0.1 mV was applied, the current was measured every second, and the resistance from Ohm's law was recorded for 90 min. We calculated mass-normalized sheet resistances by calculating sheet resistances and multiplying them with the weight of the prints from gravimetry. More details on the mass-normalized sheet resistance are given in the beginning of Section 3.1.

X-ray diffraction (XRD) measurements were performed on either 50 mg of fresh powder or the equivalent of powder scraped off from 3 heat-treated samples using a D8 advance diffractometer (Bruker, Germany) equipped with a copper source that emitted CuKα radiation (λ = 1.54060, 40 kV, 40 mA) that we recorded within the 2θ range from 10° to 80°.

Energy-dispersive X-ray spectroscopy was performed using Noran System 7 X-ray Microanalysis System (Thermo Scientific, Germany) mounted inside an SEM (same SEM as described at the start of this section). Three particles per sample were chosen from top-view SEM images at a magnification of 15 000×. X-ray spectra were recorded with a zoom-in on the chosen particles at a magnification of 400 000×, at a spot size of 4, and an acceleration voltage of 15 kV, and the ratio of the K_α oxygen: K_α copper was determined. We report average ratios calculated from the three particles to assess the amount of copper oxide formed during heat treatments.

3 Results and discussion

3.1 Sintering silver-coated copper particles

We studied the sintering of printed layers of commercial, silver-coated copper microparticles. Electrical characterization of prints is typically done by first determining the sheet resistance,

$$R_{\mathrm{sh}} = \frac{\pi}{\ln(2)} \cdot \frac{\Delta V}{I}, \tag{1}$$

where ΔV and I are the potential difference and current between two points of a thin sheet with constant thickness. The sheet resistance is then commonly used to obtain the effective resistivity,

$$\rho = R_{\mathrm{sh}} \cdot t \tag{2}$$

where t is the printed film thickness. The resulting resistivity ρ is an apparent, average value that treats the sheet as a homogeneous conductor.

Note that ρ obtained in this way contains little information on the amount of silver in the sheet. A printed metal layer with a porosity of 10% (layer A) can have the same resistivity as a layer with a porosity of 40% (layer B) although it contains 1.5 times more metal. This makes it more difficult to compare the amount of metal that has been used and its ecological and economical implications.

A suitable way to directly consider the metal content is to use a mass-normalized sheet resistance,

$$R_{m/\mathrm{sh}} = m \times R_{\mathrm{sh}} \tag{3}$$

with m the metal mass of the printed layer. Just like ρ, $R_{m/\mathrm{sh}}$ is a material property that is independent of the layer thickness. Its lowest possible value, $R_{m/\mathrm{sh,Cu}}$ = 0.045 mΩ sq^{-1} g, is reached when the layer reaches the conductivity of bulk copper. In the following, we provide $R_{m/\mathrm{sh}}$ throughout because it directly shows how to minimize the required amount of metal to obtain maximal conductivities at low temperatures in ambient air.

We used spherical particles (Cu@Ag–S) with average diameters of 1.5, 3, and 5 μm, and flake-like particles (Cu@Ag–F) with an average diameter of 3 μm. Their copper cores were coated with 10 weight percent of silver per total powder mass *via* electroless plating during production: Cu@Ag–S with 1.5, 3, and 5 μm diameter had silver shell thicknesses of 40.8, 50.5, and 63.7 nm, Cu@Ag–F had a thickness of 31.3 nm (see Fig. S1 in the ESI†). We added L-ascorbic acid (AA) to all

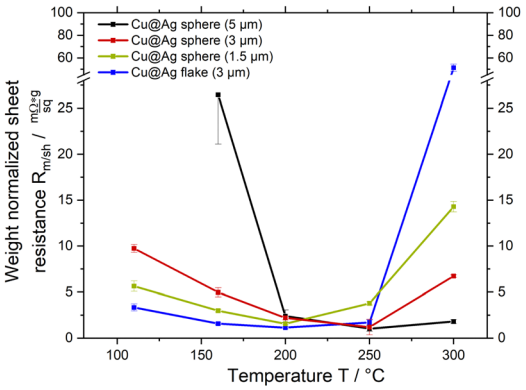

Fig. 1 Weight-normalized sheet resistances $R_{m/sh}$ of printed films of silver-copper core–shell particles after 30 min in air at temperature T. All particles contained 10 wt% of silver as shells. Spherical particles had average diameters of 1.5, 2.5, 5 µm. Flakes had an equivalent average diameter of 3 µm.

paste formulations to suppress copper oxidation during heat treatments of the prints (for more details on the suppressing effect of AA see Fig. S2 in the ESI†).[16,20]

Pastes containing Cu@Ag–S or Cu@Ag–F, ethylene glycol (EG), and AA were screen-printed on glass slides into lines and treated at 110, 160, 200, 250, and 300 °C for 30 min in air (see Fig. 1A). The degree of sintering was assessed using scanning electron microscopy (SEM) and electrical characterization.

Fig. 1A shows that all sheet resistances $R_{m/sh}$ reached minima at $T_{R,min}$ that depended on particle diameter and type: $T_{R,min} \approx 200$ °C for 1.5 µm diameter Cu@Ag–S and 3 µm Cu@Ag–F, and $T_{R,min} \approx 250$ °C for 3 and 5 µm Cu@Ag–S. The existence of an optimal sintering temperature is in stark contrast to pure silver particles, where increasing temperature at constant treatment time reduces resistance at least until 300 °C, and no resistance increase is observed when further increasing the temperature.

The decrease of $R_{m/sh}$ at 110 to 200 °C, below $T_{R,min}$, is likely caused by silver that is mobile at low temperatures. The observation is consistent with many reports on the necking of pure silver microparticles at 150 °C or below (*cf.* introduction). We argue that a similar necking occurs between the shells of silver-coated copper particles,[24,40,41] with the expected reduction of electrical resistance.

The increasing $R_{m/sh}$ at $T > T_{R,min}$ is most likely caused by the oxidation of copper. Literature reports that the silver films on copper start dewetting above 200 °C and expose copper surface.[25,26,42] Unprotected copper immediately reacts with ambient oxygen to form a native oxide layer even at room temperature. Above 150 °C, oxygen can diffuse through this native oxide, making the oxide layer thicker (*cf.* introduction). Copper oxides are insulating and likely increase $R_{m/sh}$.

We evaluated this hypothesis and studied the formation of copper oxides at $T > T_{R,min}$ using X-ray diffraction (XRD) and energy dispersive X-ray spectroscopy (EDX) in the following.

3.2 Oxidation and dewetting effects

We recorded X-ray diffraction (XRD) patterns of fresh powders and prints containing 1.5 µm Cu@Ag–S treated at 110, 200, 250, and 300 °C (Fig. 2A). Silver has characteristic diffraction reflexes at 38 and 64.5°,[26] hence the maxima observed at these positions were assigned to the silver coating of the particles.

Copper oxide peaks only formed at 250 °C and above, where Cu_2O caused reflexes at 2 − Theta = 36.4° and 61.5°.[43] They increased in intensity at 300 °C, and new peaks appeared indicating the formation of a CuO phase (2 − Theta = 66.2° and 68°). This oxidation sequence is in line with literature on copper particle oxidation in air.[14,17]

Additional energy-dispersive X-ray analysis (EDX) was used to detect oxides. The ratio of the K_α emission of oxygen and L_α emission of copper (details in the experimental section) are shown in Fig. 2B. The oxide fraction clearly correlated with the corresponding $R_{m/sh}$ at higher temperatures. It increased at 200 °C, already before XRD indicated a crystalline copper phase, suggesting the formation of amorphous oxide layers and consistent with literature.[44] The strong increase of the EDX ratio at 250 °C is consistent with the oxide seen by XRD.

The stability of silver-coated copper particles towards oxidation at elevated temperatures is limited by the dewetting of the silver coating (*cf.* introduction). We observed dewetting in electron microscopy by exploiting the backscattered electron (BSE) contrast caused by the atomic number difference between

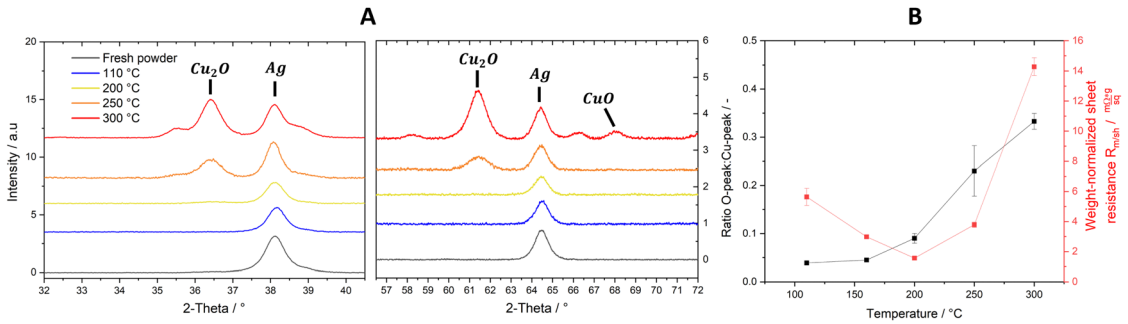

Fig. 2 Oxidation of silver-coated copper particles after heat treatments in air quantified by (A) X-ray diffraction (XRD) and (B) energy dispersive X-ray spectroscopy (EDX). (A) Prints containing 1.5 µm Cu@Ag–S treated at 110, 200, and 300 °C. Characteristic peaks of Cu, Ag CuO, and Cu_2O are indicated in the graph. (B) The temperature-dependent ratio of the K_α oxygen to the K_α copper reflex intensities (black line) and the normalized resistances $R_{m/sh}$ (red line) from EDX are shown for prints of 1.5 µm Cu@Ag–S.

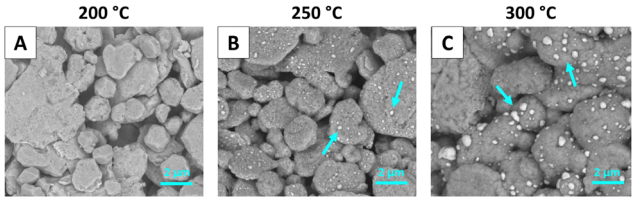

Fig. 3 Dewetting of silver coatings on core–shell copper particles. Top-view BSE images of prints containing Cu@Ag–F treated at (A) 200, (B) 250, and (C) 300 °C. Silver droplets that formed by dewetting are indicated with the blue arrows in (B) and (C).

Ag and Cu. Fig. 3 shows top-view BSE images of prints containing Cu@Ag–F treated for 30 at 200, 250, and 300 °C.

The Cu@Ag–F in Fig. 3A that were treated at 200 °C had no visible contrast on their surfaces, indicating homogeneous silver coatings. Treatment at 250 °C caused dewetting and clearly contrasting silver droplets visible in Fig. 3B. They coincided with the formation of Cu_2O detected by XRD, suggesting that dewetting preceded oxidation, as reported in literature.[14] The silver droplets were larger at 300 °C (Fig. 3C), exposing more copper, and causing stronger oxidation as detected by XRD and EDX (see above).

Having established that dewetting leads to oxidation at temperatures above $T_{R,\min}$, we now analyze in detail how different treatment temperatures (below, at, and above $T_{R,\min}$) affect $R_{m/\mathrm{sh}}$ over time and propose a mechanism for the low-temperature sintering of silver-coated particles.

3.3 Sintering mechanism of silver-coated copper particles

We followed the evolution of $R_{m/\mathrm{sh}}$ *in situ* while sintering 3 μm Cu@Ag–S. Layers with a thickness of 38.6 ± 5.3 μm were printed and dried in vacuum at room temperature for 24 h. The evolution of $R_{m/\mathrm{sh}}$ was then followed *via* two electrical contacts during 90 min at 90, 110, 160, 200, or 300 °C. Fig. 4A shows the results.

Resistances dropped to a plateau value of 3 mΩ sq^{-1} g in the first 5 min for 90 and 110 °C and remained there for the remainder of the experiment. Higher temperatures led to lower plateau values that decreased from 2 mΩ sq^{-1} g at 160 °C to 1.5 mΩ sq^{-1} g at 200 °C and 250 °C. At 300 °C, above $T_{R,\min}$, $R_{m/\mathrm{sh}}$ reached a minimum after 3 min and then increased linearly during the entire temperature treatment.

The reduction of $R_{m/\mathrm{sh}}$ in the range of 110 °C to 250 °C suggests the formation of silver necks that are connecting the particles. Scanning electron microscopy (SEM) images of a cross-section taken after 90 min at 200 °C (Fig. 4B) confirmed the existence of such necks. Note that the silver shell remained continuous: no dewetting was visible at a temperature of 200 °C (see Fig. 3A).

The continuous increase of $R_{m/\mathrm{sh}}$ observed at T = 300 °C is related to silver dewetting and copper oxidation. The onset of dewetting at 250 °C leads to the formation of Cu_2O (*cf.* oxidation and dewetting effects), but not necessarily to an increase of $R_{m/\mathrm{sh}}$, as the trace for 250 °C Fig. 4A shows. The constant $R_{m/\mathrm{sh}}$ = 1.45 mΩ sq^{-1} g is likely caused by silver necks that keep the copper cores electrically contacted and are not affected by oxide formation at other, exposed parts of the spheres. This mechanism fails at 300 °C, where both copper oxidation and dewetting are more rapid. The copper cores expand upon oxidation, inducing stresses and mechanical fracture of silver necks. Concurrently, the copper–silver interface within the particles becomes insulating, reducing the conductive pathways. Other mechanisms are likely to contribute: Hai *et al.* demonstrated that the diffusion of copper through the silver coating of particles leads to the formation of pores at the copper–silver interface that reduces conductivity. Such pores formed at and above 250 °C, too (see Fig. S3 of the ESI†).

Fig. 5 summarizes the proposed sintering processes of silver-coated copper particles in air. Temperatures below 160 °C did not lend silver sufficient mobility to form sinter necks, and $R_{m/\mathrm{sh}}$ remained limited by the particle–particle contact resistances to 3 mΩ sq^{-1} g to 6 mΩ sq^{-1} g. Temperatures of 160–250 °C mobilized the silver sufficiently to form necks connecting the particles, but retained the continuity of

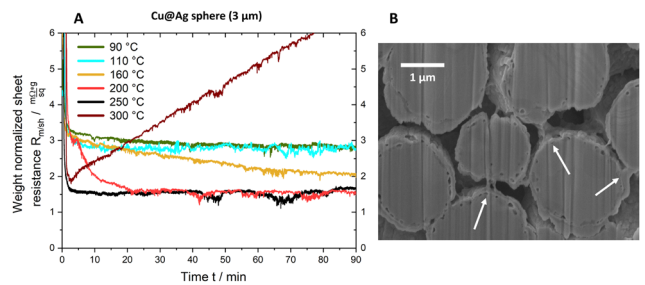

Fig. 4 (A) Resistance evolution of prints and (B) micro-structural changes at 200 °C. (A) $R_{m/\mathrm{sh}}$ as measured *in situ* while treating different prints of 3 μm -sized Cu@Ag–S treated at 90 °C to 300 °C for 90 min. The measurement started at 0 min when placing the sample on a preheated hot plate. (B) Electron microscopy of a cross-section prepared from a sample treated at 200 °C indicated silver necks (white arrows).

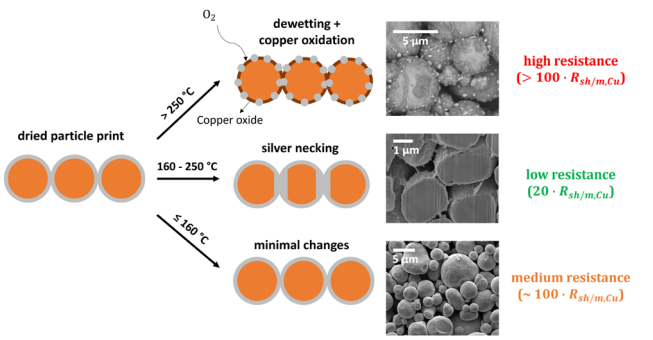

Fig. 5 Proposed sintering mechanisms of silver-coated copper particles in air. Temperatures below 160 °C hardly affected the silver coating, sheet resistances remained at $R_{m/\mathrm{sh}} \approx 10^2 \cdot R_{m/\mathrm{sh,Cu}}$, and the particles appeared unchanged in electron microscopy (shown here: 5 μm Cu@Ag–S at 110 °C). Temperatures between 160 °C and 250 °C reduced $R_{m/\mathrm{sh}}$ to $\approx 20 \cdot R_{m/\mathrm{sh,Cu}}$ and caused neck formation (shown here: 3 μm Cu@Ag–S treated at 200 °C). Temperatures above 250 °C increased $R_{m/\mathrm{sh}}$ to above $10^2 \cdot R_{m/\mathrm{sh,Cu}}$ and caused dewetting and oxidation (shown here: 5 μm Cu@Ag–S treated at 300 °C).

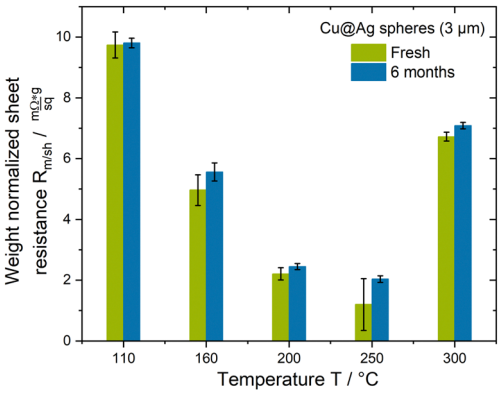

Fig. 6 Stability of weakly sintered prints under ambient conditions. $R_{m/sh}$ of prints containing 3 µm -sized Cu@Ag–S after sintering ('fresh') and after 6 months storage in laboratory air at standard conditions (*cf.* Preparation and printing of pastes.).

the shells that protect the copper from oxidation. They reduced $R_{m/sh}$ to 1 mΩ sq^{-1} g to 1.5 mΩ sq^{-1} g (6.9×10^{-5} Ω cm to 9.1×10^{-5} Ω cm). A combination of dewetting and rapid copper oxidation at temperatures above 250 °C led to a continuously increasing $R_{m/sh}$.

The mechanisms illustrated in Fig. 5 explain the optimal sintering temperature $T_{R,min}$ for the core–shell particles that does not exist for homogeneous silver spheres.

We assessed the stability of prints by storing them under ambient conditions for 6 months. Fig. 6 illustrates that the $R_{m/sh}$ of prints of 3 µm Cu@Ag–S underwent no significant changes, indicating that the samples were stable.

3.4 Recyclability

We demonstrated that prints of silver-coated copper spheres and flakes consistently decrease in electrical resistance $R_{m/sh}$ with increasing temperature until a certain temperature. Treatments at higher temperatures increased the resistance. Prints containing Cu@Ag–F resulted in the lowest $R_{m/sh}$ for treatments below 200 °C. We chose these films to study the recovery of metal powders from the prints. The redispersion of the particles could simplify the recovery and recycling of metal particles from printed electronics (*cf.* Introduction).

The cycle of making paste, printing, and recycling of metal powder is shown in Fig. 7A. We prepared prints containing Cu@Ag–F that were treated at three different temperatures. Pastes were printed on glass slides, put in a vacuum at room temperature for 2 days, 80 °C for 30 min, or 160 °C for 30 min. The $R_{m/sh}$ of these prints are shown as 'first generation' in the green bars in Fig. 7B. The prints were then mechanically removed, powder was collected, and new pastes were made from them. Lines were printed on glass slides and treated identically to the first-generation prints that they came from. The $R_{m/sh}$ for these 'second generation' prints are shown as blue bars in Fig. 7B.

The $R_{m/sh}$ of first-generation prints decreased with increasing temperature as discussed in the preceding sections. The $R_{m/sh}$ of all second-generation prints were larger than the respective first-generation prints. We propose that this degradation reflects copper exposure or thinning of the silver coating due to fracturing particle–particle contacts. Exposed and thinned silver coating causes native oxide growth at room temperature.[17–19] Second-generation prints contain more particle–particle contacts with an oxide layer that cause large contact resistances, leading to larger overall $R_{m/sh}$. This is consistent with the small increase in $R_{m/sh}$ for second-generation prints that were treated in a vacuum at room temperature. The mobility of silver at room temperature is too low for silver to migrate much, leading to a silver coating that stays intact even after recycling of the particles.

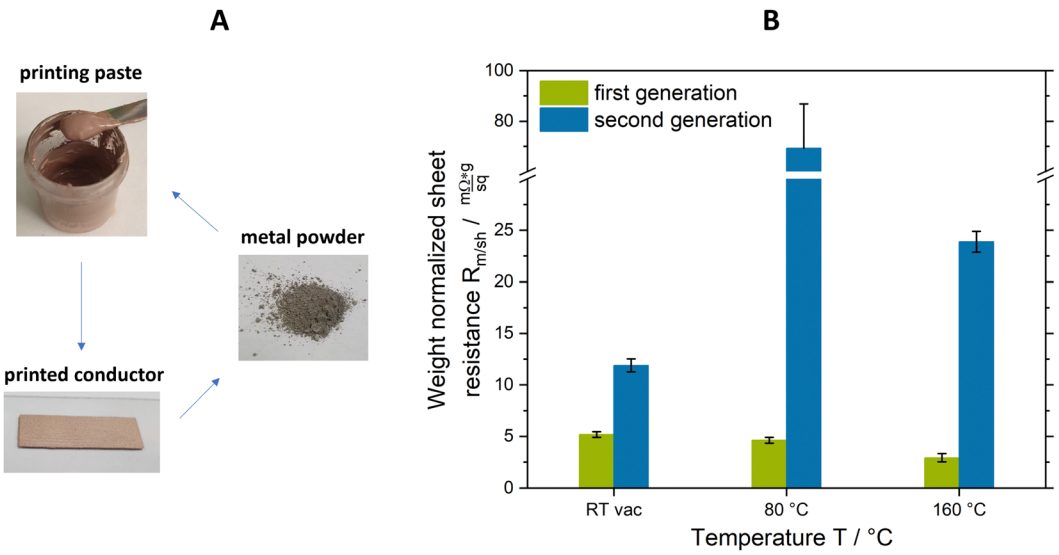

Fig. 7 Recyclability of prints of silver–copper core–shell particles after three different heat treatments. (A) Circular paste preparation, printing, and recycling. (B) Electrical performance of freshly printed Cu@Ag–F compared to prints made from recycled Cu@Ag–F after vacuum drying at room temperature for 2 days, thermal treatment at 80 °C for 30 min, and sintering at 160 °C for 30 min. Green bars indicate fresh prints and blue bars indicate recycled prints.

In summary, it was possible to recycle weakly sintered Cu@Ag–F from prints, but the performance of the material degraded. Heat treatments at 160 °C reduced $R_{m/sh}$ of the first generation to 2.9 mΩ sq^{-1} g (1.46 × 10^{-4} Ω cm) but increased $R_{m/sh}$ of the second generation of prints by a factor of 8. Limiting the first-generation treatment to room temperature increased $R_{m/sh}$ to 5.2 mΩ sq^{-1} g (2.72 × 10^{-4} Ω cm) for the first generation but limited the increase in the second generation to a factor of 2.

4 Conclusion

We prepared conductive films from silver-coated copper spheres (Cu@Ag–S) and flakes (Cu@Ag–F) and treated them at low temperatures in air. The mass-normalized sheet resistances $R_{m/sh}$ of all prints decreased with increasing temperatures below $T_{R,min}$ that depended on the particle type and reached a minimal $R_{m/sh}$ of 1 mΩ sq^{-1} g to 1.5 mΩ sq^{-1} g (6.9 × 10^{-5} Ω cm to 9.1 × 10^{-5} Ω cm). Treatments at $T > T_{R,min}$ increased $R_{m/sh}$.

A combination of *in situ* electrical characterization and cross-section SEM imaging revealed that the dropping of $R_{m/sh}$ below $T_{R,min}$ is a result of low-temperature silver sintering. A pronounced drop in $R_{m/sh}$ appeared only above 160 °C. This characteristic drop was linked to the formation of silver necks that were identified by cross-sectional SEM imaging.

Dewetting and oxidation were identified as the mechanisms increasing $R_{m/sh}$ at $T > T_{R,min}$. BSE imaging revealed the onset of silver dewetting at 250 °C. Exposed copper areas and locally thinning silver coatings enabled the formation of Cu_2O as confirmed by XRD. The combination of rapid oxidation of exposed copper and the dewetting of particles led to a continuously increasing $R_{m/sh}$ at and above 250 °C.

The choice of sintering temperature is crucial to obtaining highly conductive prints of silver-coated copper particles. Temperatures below 160 °C do not lead to sintering and limit $R_{m/sh}$ to 3 mΩ sq^{-1} g to 6 mΩ sq^{-1} g. Temperatures above 250 °C increase $R_{m/sh}$ by oxidation and reduced silver necking. Sintering at 160 °C to 250 °C minimizes $R_{m/sh}$ to minimal values in the range of 1 mΩ sq^{-1} g to 1.5 mΩ sq^{-1} g (6.9 × 10^{-5} Ω cm to 9.1 × 10^{-5} Ω cm).

We tested the recovery of weakly sintered prints of silver-coated copper particles. The first-generation prints were treated and removed from the substrate to recover powders that were formulated as second-generation pastes. The second-generation prints consistently had a higher $R_{m/sh}$ than the respective first-generation prints. We found a trade-off: room temperature drying of prints limited electrical degradation after recycling to a factor of 2 while 160 °C let to a factor of 8. Depending on the application, it is possible to enable recycling by minimizing sintering temperature at the cost of conductivity.

Author contributions

David van Impelen wrote the original draft of the manuscript and performed all experiments. All authors took part in the conceptualization, reviewing and editing of the manuscript. Tobias Kraus and Lola González-García were leading the supervision. Tobias Kraus was responsible for the funding acquisition and resources.

Data availability

The data that support the findings of this study are available from the corresponding author, Tobias Kraus, upon reasonable request.

Conflicts of interest

There are no conflicts of interest to declare.

Acknowledgements

We acknowledge Dominik Perius for his preparation of printed layer cross-sections *via* FIB-SEM and Albenc Nexha for X-ray diffraction analyses. This work was supported by the German Federal Foundation for the Environment (DBU). We thank Jochen Wahl (CEO of GSB Wahl GmbH) for his contributions to discussions on low-impact conductive pastes.

References

1 D. Lide, *CRC Handbook of chemistry and physics*, 2007.
2 D. Pletcher and F. C. Walsh, *Silver Chemistry*, Wiley, Chichester, UK, 1st edn, 1992.
3 S. A. Paknejad and S. H. Mannan, *Microelectron. Reliab.*, 2017, **70**, 1–11.
4 K. Rajan, I. Roppolo, A. Chiappone, S. Bocchini, D. Perrone and A. Chiolerio, *Nanotechnol. Sci. Appl.*, 2016, **9**, 1–13.
5 Silver Institute, Silver Market Interim Report 2023, 2023, **https://www.silverinstitute.org/wp-content/uploads/2023/11/SilverMarket2023_interim-report.pdf**.
6 M. J. Eckelman and T. E. Graedel, *Environ. Sci. Technol.*, 2007, **41**, 6283–6289.
7 J. Kwon, C. DelRe, P. Kang, A. Hall, D. Arnold, I. Jayapurna, L. Ma, M. Michalek, R. Ritchie and T. Xu, *Adv. Mater.*, 2022, **34**, 2202177.
8 W. M. Haynes, *CRC Handbook of Chemistry and Physics*, 2016, p. 2670.
9 Daily Metal Price, Daily Metal Price, 2022, **https://www.dailymetalprice.com/metalprices.php?c=cuu=ozd=10**.
10 USGS (United States Geological Survey), 2022.
11 International Copper Study Group (ICSG), Long Term Availability of Copper, 2022, **https://icsg.org/long-term-availability-of-copper/**.
12 D. Tomotoshi and H. Kawasaki, *Nanomaterials*, 2020, **10**, 1689.
13 M. Nishimoto, R. Tokura, M. T. Nguyen and T. Yonezawa, *Mater. Trans.*, 2022, **63**, 663–675.

14 S. Choudhary, J. V. N. Sarma, S. Pande, S. Ababou-Girard, P. Turban, B. Lepine and S. Gangopadhyay, *AIP Adv.*, 2018, **8**, 055114.
15 H. Wieder and A. W. Czanderna, *J. Phys. Chem.*, 1962, **66**, 816–821.
16 N. L. Pacioni, V. Filippenko, N. Presseau and J. C. Scaiano, *Dalton Trans.*, 2013, **42**, 5832–5838.
17 C. Gattinoni and A. Michaelides, *Surf. Sci. Rep.*, 2015, **70**, 424–447.
18 P. Keil, D. Luetzenkirchen-Hecht and R. Frahm, *AIP Conf. Proc.*, 2007, **882**, 490–492.
19 J. J. D. León, D. M. Fryauf, R. D. Cormia and N. P. Kobayashi, *Low-Dimensional Materials and Devices 2016*, 2016, p. 99240O.
20 Y. Gao, W. Li, C. Chen, H. Zhang, J. Jiu, C.-F. Li, S. Nagao and K. Suganuma, *Mater. Design*, 2018, **160**, 1265–1272.
21 Y. Zhang, P. Zhu, G. Li, T. Zhao, X. Fu, R. Sun, F. Zhou and C.-P. Wong, *ACS Appl. Mater. Interfaces*, 2014, **6**, 560–567.
22 M. Shlomo, G. Michael and K. Alexander, *Materials*, 2010, **3**, 4626–4638.
23 E. B. Choi and J.-H. Lee, *Appl. Surf. Sci.*, 2019, **480**, 839–845.
24 X. Yu, J. Li, T. Shi, C. Cheng, G. Liao, J. Fan, T. Li and Z. Tang, *J. Alloys Compd.*, 2017, **724**, 365–372.
25 H. T. Hai, H. Takamura and J. Koike, *J. Alloys Compd.*, 2013, **564**, 71–77.
26 J. H. Kim and J.-H. Lee, *Jpn J. Appl. Phys.*, 2016, **55**, 06JG01.
27 A. Pajor-Świerzy, Y. Farraj, A. Kamyshny and S. Magdassi, *Colloids Surf., A*, 2017, **521**, 272–280.
28 A. Pajor-Świerzy, Y. Farraj, A. Kamyshny and S. Magdassi, *Colloids Surf., A*, 2017, **522**, 320–327.
29 A. Pajor-Świerzy, K. Szczepanowicz, A. Kamyshny and S. Magdassi, *Adv. Colloid Interface Sci.*, 2022, **299**, 102578.
30 C.-K. Kim, G.-J. Lee, L. Min Gu and C. K. Rhee, *Powder Technol.*, 2014, **263**, 1–6.
31 N. R. Kim, Y. Lee, C. Lee, J. Koo and H. Lee, *Nanotechnology*, 2016, **27**, 345706.
32 C. Lee, N. R. Kim, J. Koo, Y. Lee and H. Lee, *Nanotechnology*, 2015, **26**, 455601.
33 A. Titkov, O. Logutenko, A. Vorobyov, E. Gerasimov, I. Shundrina, N. Bulina and N. Lyakhov, *Colloids Surf., A*, 2019, **577**, 500–508.
34 Y. Zhang, P. Zhu, G. li, Z. Cui, C. Cui, K. Zhang, J. Gao, X. Chen, G. Zhang, R. Sun and C. Wong, *ACS Appl. Mater. Interfaces*, 2019, **11**, 560–567.
35 S. Kim, M. Kim and J.-H. Lee, *J. Mater. Sci.: Mater. Electron.*, 2020, **27**, 16720–16727.
36 G. Yang, P. Wang, Y. Liu, S. Lu, B. Luo, T. Lai, S. Ta, T. Lin, J. Luo, Y. Zhang and C. Cui, *J. Alloys Compd.*, 2022, **923**, 166271.
37 W. Yang, W. Zhu, X. Wang, S. Hu, P. Cui, Y. Fang, Z. Li, F. Qi, H. Cao, H. Xu and M. Li, *Mater. Lett.*, 2023, **357**, 135675.
38 M. Won, D. Kim, H. Yang and C. Oh, *Energies*, 2023, **16**, 5419.
39 Y. Tian, Z. Jiang, C. Wang, S. Ding, J. Wen, Z.-Q. Liu and C. Wang, *RSC Adv.*, 2016, **6**, 91783–91790.
40 M. I. Kim and J.-H. Lee, *J. Mater. Res. Technol.*, 2021, **14**, 1724–1738.
41 Y. Kim, E. B. Choi and J.-H. Lee, *Appl. Surf. Sci.*, 2023, **640**, 158326.
42 M. Grouchko, A. Kamyshny and S. Magdassi, *J. Mater. Chem.*, 2009, **19**, 3057–3062.
43 A. Zhakypov, R. Nemkayeva, Y. Yerlanuly, M. Tulegenova, B. Kurbanov, M. Aitzhanov, A. Markhabayeva and M. Gabdullin, *Sci. Rep.*, 2023, **13**, 15714.
44 S. Choudhary, J. V. N. Sarma, S. Pande, S. Ababou-Girard, P. Turban, B. Lepine and S. Gangopadhyay, *AIP Adv.*, 2018, **8**, 055114.